Origin of perpendicular magnetic anisotropy and large orbital moment in Fe atoms on MgO

S. Baumann,[1,2] F. Donati,[3] S. Stepanow,[4] S. Rusponi,[3] W. Paul,[1]
S. Gangopadhyay,[1,5] I. G. Rau,[1] G. E. Pacchioni,[3] L. Gragnaniello,[3]
M. Pivetta,[3] J. Dreiser,[3,6] C. Piamonteze,[6] C. P. Lutz,[1] R. M. Macfarlane,[1]
B. A. Jones,[1] P. Gambardella,[4] A. J. Heinrich,[1] and H. Brune[3]

[1]*IBM Almaden Research Center, 650 Harry Road, San Jose, CA 95120, USA*
[2]*Department of Physics, University of Basel, Klingelbergstrasse 82, CH-4056 Basel, Switzerland*
[3]*Institute of Condensed Matter Physics, École Polytechnique Fédérale de Lausanne (EPFL), Station 3, CH-1015-Lausanne, Switzerland*
[4]*Department of Materials, ETH Zürich Hönggerbergring 64, CH-8093 Zürich, Switzerland*
[5]*Department of Physics, University of California, Davis CA 95616, USA*
[6]*Swiss Light Source (SLS), Paul Scherrer Institute (PSI), CH-5232 Villigen PSI, Switzerland*

SAMPLE PREPARATION

The sample preparation was done the same way in independent vacuum systems for the STM and XMCD experiments. First, the sample was cleaned by repeated sputter and annealing cycles of the Ag(100) single crystal, until an atomically clean surface was achieved, as verified by Auger spectroscopy and spot checked by STM imaging. Second, the Mg was evaporated from a crucible in an O_2 atmosphere of $p_{O_2} = 10^{-6}$ mbar. We used growth rates of approximately 1 monolayer (ML) per minute at a sample temperature of typically 320 °C. Typical morphologies of the MgO films obtained using this procedure are shown in [33]. The samples covered with the thin MgO films on Ag were then transferred without breaking the vacuum into a low-temperature system. The Fe atoms were evaporated from a high purity rod onto the sample kept at about 5 - 10 K. Measurements were performed at 0.6 K in the STM and 2.5 K in the XMCD and in magnetic fields up to 6.8 T.

STM METHODS

All STM measurements were performed at the IBM Almaden Research Center in a low-temperature ultra-high vacuum system [35]. Upon imaging, the Fe atoms' appearance is almost independent of the local MgO thickness for 1 – 3 ML in the STM measurements, where the thickness of the different MgO islands was determined according to [33] by imaging the area at high bias voltage and thereby removing the atoms from the surface. The spin-excitation experiments used a DC voltage between the sample and the STM tip (positioned over the Fe atom) while measuring conductance with a lock-in technique with 70 to 150 μV, 806 Hz AC excitation. When the applied bias matches a magnetic excitation in the atom a second conductance channel opens up which is visible as a step-wise increase in the measured differential conductance symmetric around zero-bias at the excitation voltage [35]. For the measurements with spin-polarized tips, magnetic atoms were transferred to the tip apex and a magnetic field was applied to orient the magnetization of the tip [57].

Fits to IETS data

We fitted the observed step in dI/dV with the expected thermally broadened inelastic electron tunneling functional form [36] to extract the excitation threshold and the step-

width. Small differences between the absolute conductance are due to small experimental variations in the height of the tip above the atom. To make the different magnetic field data directly comparable, the conductance step is scaled to match their heights. The step height, position, step width and vertical offset are fitting parameters. For the smallest AC excitation amplitudes, the fitted width at 0 T is 0.73 mV. This width corresponds to $5.5\,k_{\mathrm{B}}T$ in the case of a thermally broadened transition, resulting in $T = 1.54$ K. The extracted equivalent temperature is larger than the 0.6–0.7 K measurement temperature. We have excluded the applied AC voltage as a possible broadening source: reducing the modulation amplitude does not affect the transition width. The nature of this broadening is not yet understood. Lifetime broadening is not expected since the lifetimes of more than 1 ns inferred from the observation of the ≈ 105 mV transition imply lifetime broadening of less than $1\,\mu$V. The 2 T data was also fitted with a single IETS step which resulted in an even wider step of 1.23 mV. This 2 T step should potentially be fitted with a double step, however, the splitting between the two steps is not sufficiently large to resolve them.

The positions of the two separate steps at 4 and 6 T are fitted with the sum of two inelastic electron tunneling functional forms of the same width. Figure S1 shows how such a fit to the 6 T spectrum looks like for 3 different widths. The heights and positions of the steps were allowed to vary independently. Interestingly, the width of the two separate steps at 6 T is 0.65 mV, which is smaller than the 0 T step width. We ensure that the extracted step positions are robust against changes in the fitting parameters by fitting the double IETS step for several different fixed step widths ranging from 0.3 to 0.65 mV. The resulting step positions are shown in Fig. S1. The position of the lower-energy step varies by 0.30 mV and the position of the higher-energy step by 0.01 mV in the given range. For the extracted step used in the main text the fit width employed is 0.3 mV which results in a difference between the two step positions of 1.9 ± 0.3 mV at 6 T.

Magnetic field dependence with in-plane field

For most of the STM experiments the magnetic field was applied out-of-plane. To verify the out-of-plane uniaxial anisotropy observed in XAS/XMCD measurement, we here compare a set of measurements with in-plane as well as with out-of-plane magnetic field (Fig. S2). When the magnetic field is applied in-plane no shift of the IETS step is observable, while

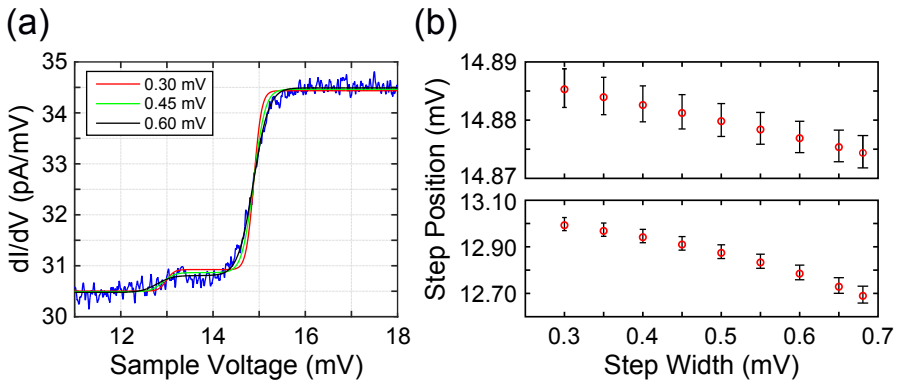

Figure S1. (a) Zoom-in on the Fe IETS step at 6 T (blue) and three fits with a double step of fixed width of 0.3 mV (red), 0.45 mV (green) and 0.6 mV (black) ($I = 1$ nA, $V = 30$ mV). (b) The position of the low energy (bottom panel) and high energy step (top panel) extracted from the fit to the 6 T data, as a function of fixed IETS width.

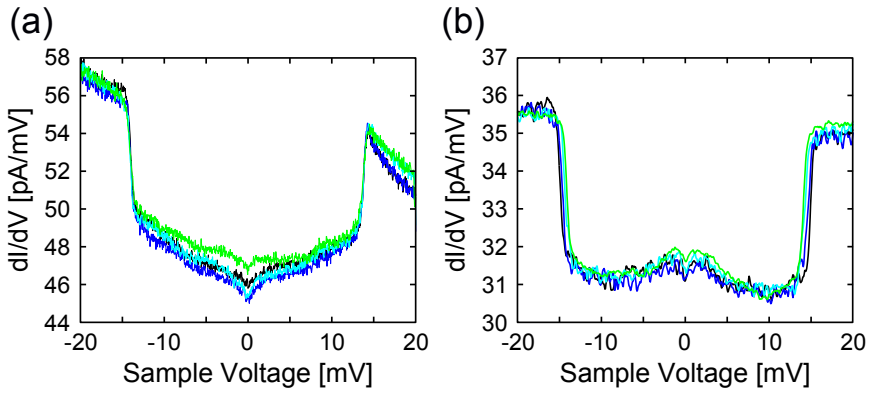

Figure S2. Energy shift of the inelastic excitations of Fe on MgO in an in-plane (a) and out-of-plane (b) magnetic field (green: 0 T, cyan: 2 T, blue: 4 T and black 6 T). The steps only change in the out-of-plane field indicating an uniaxial anisotropy in that out-of-plane direction. The vertical shift among the curves around the zero bias can occur due to slight variations in the tip height when opening the feedback loop. [(a) $I = 0.1$ nA, $V = 100$ mV; (b) $I = 1$ nA, $V = 30$ mV]

for the out-of-plane direction the IETS step moves due to the applied field (only the higher-energy step is readily visible with these measurement conditions). The absence of energy shift under the effect of an in-plane magnetic fields is indicative of an out-of-plane easy axis. This also confirms that the two lowest states behave, to very good approximation, as a pure non-Kramers' doublet, for which a zero-response to transverse field is expected [37].

DETAILS OF DFT CALCULATIONS

To model the periodic 2D slab geometry, we used spin-polarized density functional theory (DFT) with plane wave basis, as implemented in Quantum ESPRESSO [38] and Wien2k [39]. We used the generalized gradient approximation (GGA) and included on-site Coulomb interaction (U = 3.2 eV) for the d-states of Fe. The value of U is obtained using a linear response approach implemented in Quantum ESPRESSO [52]. We optimized the geometry of a slab of six atomic layers of Ag, in which the lower three are kept fixed at bulk Ag values. On top of the Ag layers we added a layer of MgO where the O atoms are on-top of the Ag atoms as referred by previous DFT calculations [28, 40]. For the calculation, we implemented 8 effective atomic layers of vacuum above the slab. We added Fe on two of the three possible adatom sites on the MgO surface, namely on top of O and on a bridge site between two O and two Mg atoms and optimized the whole Fe/MgO/Ag system. The adsorption on the top of Mg site was not considered as it was proven to be strongly unfavored for Fe atoms at the surface of bulk MgO(100)[41], as well as for Co and Ni adatoms on 1 ML MgO/Ag(100) [28, 42].

The O top site is the most energetically favored site with an energy difference of 0.4 eV/adatom over the bridge site, indicating that Fe prefers to adsorb on the O top site. The obtained optimized geometry shows that the Fe atom stays 186 pm above the O atom and O-Mg distance is 217 pm. The calculation also shows that the oxygen directly underneath the Fe is displaced by 40 pm upwards. We additionally performed spin-orbit coupling calculations using Wien2k, where we added an orbital polarization on Fe 3d instead of the on-site Coulomb interaction U. This approach with orbital polarization was applied successfully for bulk calculations of different transition metal atoms [43–45]. In our calculations this is the first time this approach is used on single atoms on a surface. With this method we find an orbital moment of $\approx 0.7\,\mu_{\mathrm{B}}$ on Fe and a spin moment of $0.1\,\mu_{\mathrm{B}}$ on the oxygen atom sitting below Fe, at a single monolayer of MgO. We note that the orbital moment is known to be underestimated in this new DFT technique and future research is needed to understand this discrepancy [45].

Table S-I. Löwdin charge (in units of e) and spin magnetic moments (in μ_B) for Fe and O atoms at the MgO/Ag(100) surface. The remaining unbalanced charge ($+0.1\,e$) is distributed between four Mg atom coordinated with O.

	Fe					O			
	Löwdin charge			Spin moment		Löwdin charge			Spin moment
	Atomic	Above O	Diff.			Atomic	Below Fe	Diff.	
$4s$	2	0.73	+1.27	0.13	$2s$	2	1.64	0.36	0.02
$4p$	0	0.37	-0.37	0.16	$2p$	4	4.88	-0.88	0.09
$3d$	6	6.46	-0.46	3.43					
Total			+0.44	3.72	Total			-0.54	0.11

Löwdin charge analysis

We used the Löwdin population analysis to determine the charges on the different atoms in the system. The analysis shows an overall positive charge of ($+0.44\,e$) on the Fe atom. Note that Co on the same binding site is nearly charge neutral [28]. The observed total charge on the Fe is a result of the net charge obtained from $3d$, $4s$ and $4p$ orbitals. The Fe $4s$ ($+1.27\,e$) orbital is exchanging electrons with the O $2p_z$ ($-0.88\,e$) orbital which is the origin of a strong σ bond. Additionally, both the Fe $3d$ and $4p$ orbitals are accepting electrons from the O $2s$, which gives rise to a weak π acceptance between Fe and O (see table S-I). The Fe atom influences mainly the charges on the nearest neighbor atoms, while the next nearest neighbors remain almost unaffected in comparison to calculations of bare MgO/Ag(100).

XAS AND XMCD METHODS

The x-ray experiments were performed at the X-Treme beamline of the Swiss Light Source (SLS) [53] using circularly polarized light at a temperature of 2.5 K and in magnetic fields up to 6.8 T. The MgO coverage, calibrated by in-situ STM images, was chosen to be between 2 and 4 MLs in order to ensure the complete coverage of Ag by MgO. Fe was deposited directly

in the XMCD cryostat from high-purity rods (99.995%) using an e-beam evaporator on the sample kept at about 4 K and in a pressure below 5×10^{-11} mbar. The Fe coverage was calibrated using the absorption intensity at the Fe L_3 edge measured on reference samples for which the Fe coverage was determined by STM. The spectra were recorded in the total electron yield (TEY) mode with the magnetic field applied colinear with the photon beam at normal ($\theta = 0°$) and grazing incidence ($\theta = 60°$). The XMCD signal is the difference of XAS recorded for parallel (I^+) and antiparallel (I^-) alignment of the photon helicity with the applied magnetic field. Due to the small coverage, the Fe absorption intensity is small and superimposed on a large background signal originating mostly from the excitation of the Ag M-edges. This background was measured prior to the deposition of Fe and subsequently subtracted from the XAS in order to facilitate the analysis.

XAS measurements of metal atoms on thin insulating layers present technical challenges related to the low concentration of the atoms to be probed as well as to the x-ray induced desorption of the adatoms [28, 46]. Similarly to Co atoms, we found that the XAS intensity of Fe quickly decreased as a function of time due to exposure to the x-ray beam, by about 20% in 120 s, which is the time required to measure a single absorption scan. When moving the x-ray beam over the sample to a new region, which had not been exposed before, the XAS and XMCD intensities recovered to the original value. For this reason, every x-ray absorption spectrum was measured on a different region of the sample using a defocused x-ray beam spot size of 1.2 mm$\times$ 0.3 mm. The XAS shown in the manuscript are the average of two I^+ and two I^- spectra recorded over four different regions. In order to obtain a more precise estimation of the magnetic moments from the sum rules [47, 60, 61], a dedicated sample was measured with the specific aim to accumulate spectra in saturation conditions ($\theta = 0°, B = 6.8$ T), allowing a better background subtraction and signal-to-noise ratio.

The sum rules yield a large orbital magnetic moment of $\langle L_z \rangle \, \mu_\mathrm{B} = 1.74 \pm 0.11 \, \mu_\mathrm{B}$ and an effective spin magnetic moment of $\langle 2S_z + 7T_z \rangle \, \mu_\mathrm{B} = 2.46 \pm 0.11 \, \mu_\mathrm{B}$ (assuming 3.9 d holes, as found in the multiplet calculations; T_z is the out-of-plane projection of the atomic magnetic dipole moment), both values in fair agreement with the corresponding $\langle L_z \rangle \, \mu_\mathrm{B} = 1.25 \, \mu_\mathrm{B}$ and $\langle 2S_z + 7T_z \rangle \, \mu_\mathrm{B} = 2.11 \, \mu_\mathrm{B}$ from multiplet calculations. In the absence of an angular-dependent measurement of the effective spin moment, we could not determine an experimental value of $\langle S_z \rangle$ [48], thus preventing a direct comparison with the DFT results.

Magnetization curves versus applied field (Fig. 2C, main text) were measured at normal

incidence by saturating the magnetic moment at 6.8 T and recording a pair of spectra I^+ and I^-, with each spectrum taken on a different sample position. The values of the magnetization are obtained from the maximum of the XMCD signal measured at 704 eV. Because of the need to measure spectra at different points and the larger footprint of the x-ray beam at $\theta = 60°$, it was not possible to measure the magnetization versus field at grazing incidence.

MULTIPLET CALCULATIONS

The XAS simulations are based on an atomic multiplet model that takes into account the electron-electron interaction among *d*- and *p*-electrons using rescaled Slater-Condon integrals, and the atomic spin-orbit interaction [49]. The atomic environment is simulated by the crystal field potential generated by the surrounding bonding atoms. The finite overlap of the metal wavefunctions with the ligand atoms (covalency) as well as charge fluctuations in the initial and final states are described by extending the atomic multiplet model to configurational interaction. In such a scheme, in addition to the correlated state of the central atom one considers an additional (delocalized) state or band outside the atom that is generally localized on the ligands [50]. The coupling of this state to the central atom is enabled via a hopping term that effectively annihilates an electron or hole at the ligand orbital and recreates it at the atom site.

The intensity I of the x-ray absorption spectra is calculated using the dipole approximation within Fermi's Golden rule. At finite temperature, the population of excited states of the initial state configuration is also taken into account by considering transitions from Boltzmann weighted initial states. In order to compare the calculated spectra with the experimental ones, the transition amplitudes at the $L_{2,3}$ edges are broadened by a Lorentzian function with FWHM of 0.15 eV. The spectrum is further broadened by a Gaussian function with 0.15 eV FWHM to account for the experimental energy resolution.

The ligand field and hopping parameters as well as the charge transfer energy are determined by systematically varying their values in increasingly narrow energy intervals, starting from an educated guess of their range. The Slater-Condon integrals are rescaled by 75 % because of the overestimation of the Hartree-Fock value and a further reduction due to chemical bonding. The value of the one-electron spin-orbit coupling constant of Fe is taken

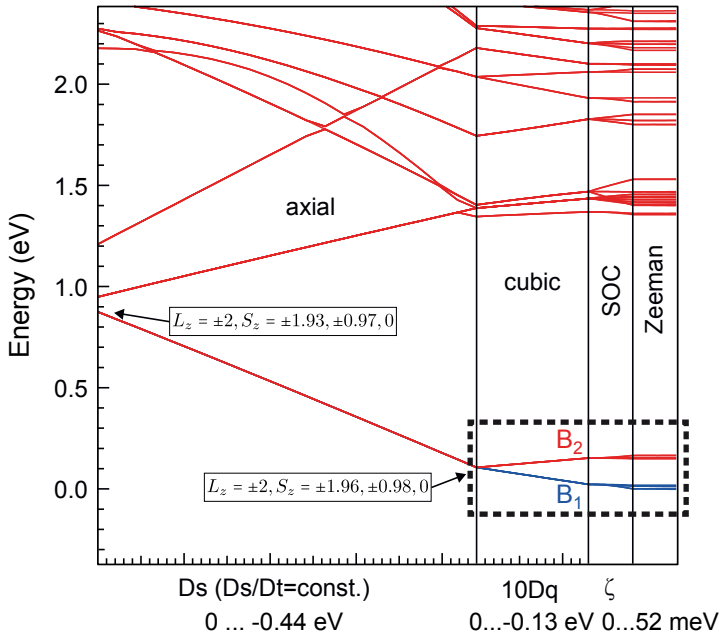

Figure S3. Level splitting under the effect of crystal field parameters Ds (with a fixed ratio Ds/Dt) and $10Dq$, the spin orbit coupling ζ and Zeeman energy. The dashed box indicates the parameter space magnified in Fig. 3 of the main text.

to be 52 meV and 45 meV for the d^6 and d^7 configurations, respectively. The charge transfer energy between the initial state configurations $\Delta_i = E(d^7) - E(d^6)$ was set to 0.5 eV, whereas for the final state it was set to $\Delta_f = -0.5$ eV. Charge transfer between O and Fe is allowed via hopping to the out-of-plane a_1 (d_{z^2}) orbital, with the hopping parameter $t = 0.85$ eV. Best agreement with the XAS spectra shown in Fig. 2 of the main text was obtained using the uniaxial crystal field parameters $Ds = -0.44$ eV and $Dt = -0.015$ eV, and the cubic term $10Dq = -0.13$ eV [51].

The overall splitting of the multiplets under the effect of the crystal field parameters, the spin orbit coupling ζ and the Zeeman splitting is shown in Fig. S3. Details on the splitting of the lowest ten levels are reported in Fig. 3 of the main text.